Received 9 June 2025; accepted 1 July 2025. Date of publication 10 July 2025; date of current version 6 November 2025.

Digital Object Identifier 10.1109/OJAP.2025.3587403

Multiband Measurement-Based Characterization of Building Materials

SILVI KODRA[1], ELENA BERNARDI[1] (Graduate Student Member, IEEE), NICOLÒ CENNI[1] (Graduate Student Member, IEEE), JIAHAO HU[2], MARINA BARBIROLI[1], FRANCO FUSCHINI[1], ENRICO MARIA VITUCCI[1] (Senior Member, IEEE), JOSE-MARIA MOLINA GARCIA-PARDO[3], MARÍA-TERESA MARTÍNEZ-INGLÉS[4], SANA SALOUS[2] (Senior Member, IEEE), AND VITTORIO DEGLI-ESPOSTI[1] (Senior Member, IEEE)

[1]Department of Electrical, Electronic and Information Engineering "G. Marconi," CNIT, University of Bologna, 40126 Bologna, Italy
[2]Department of Engineering, Durham University, DH1 3LE Durham, U.K.
[3]Departamento de Tecnologías de la Información y las Comunicaciones, Universidad Politécnica de Cartagena, 30202 Cartagena, Spain
[4]Ministerio de Defensa-Universidad Politécnica de Cartagena, Departamento de Ingeniería y Técnicas Aplicadas, Centro Universitario de la Defensa, San Javier Air Force Base, 30720 Santiago de la Ribera, Spain

CORRESPONDING AUTHOR: S. KODRA (e-mail: silvi.kodra2@unibo.it)

This work was supported in part by the European Union—Next Generation EU under the Italian National Recovery and Resilience Plan (NRRP), Mission 4, Component 2, Investment 1.3, CUP J33C22002880001, partnership on "Telecommunications of the Future" (Program "RESTART") under Grant PE00000001, in part by the EU Project 6G-SHINE (6G Short Range Extreme Communication in Entities), Horizon Europe Program under Grant 101095738, in part by the EU COST Action INTERACT (Intelligence-Enabling Radio Communications for Seamless Inclusive Interactions) under Grant CA20120, in part by the Ministerio de Ciencia e Innovación of Spanish Government under the National Grant PID2022-136869NB-C32, and in part by the U.K. Engineering and Physical Sciences Research Council (EPSRC) Funding Grant, TRACCS, under Grant EP/W027151/1.

ABSTRACT Millimeter-wave and sub-THz wireless communications promise high data rate and low-latency transmission for both indoor and outdoor short-range applications, but their deployment faces challenges due to the high isotropic path loss and severe obstacle penetration attenuation. The upper mid-band - also known as "FR3", between 7 and 24 GHz - is gaining significant attention for 6G applications, but the corresponding propagation and material characteristics still remain scarcely investigated. Therefore, thorough studies of radio-wave interaction with the most common construction materials in the cited frequency bands are very important for the design and deployment of next-generation wireless systems. The present study investigates the attenuation and scattering behaviors of some of the most common construction materials at frequencies ranging from 10 to 153 GHz, using proper measurement setups and post-processing procedures. Our findings can contribute to the design of future communication systems and to the calibration of propagation simulators that are necessary for their optimization and deployment in real-life scenarios.

INDEX TERMS Propagation measurements, FR3, mm-wave, sub-THz, building materials, transmission loss, scattering, 6G.

I. INTRODUCTION

MILLIMETER-WAVE (mmWave) and sub-THz communication systems enable high data rates and low latency, but are significantly affected by propagation challenges, particularly in obstructed environments. Although research on these high-frequency bands continues, the upper-mid-band spectrum (7–24 GHz, known as FR3) has emerged as a promising candidate for early 6G applications [1]. In this context, compatibility studies are being considered under WRC-27 Agenda Item 1.7 [2]. Indoor and micro-cellular communications play a vital role in modern wireless networks, as most of the data traffic originates indoors. A fundamental aspect of system design and coverage planning is understanding how radio waves interact with building materials [3]. While free-space, isotropic path loss increases with frequency, material-induced attenuation is less predictable [4]: some materials exhibit relatively low losses even at high frequencies, challenging common

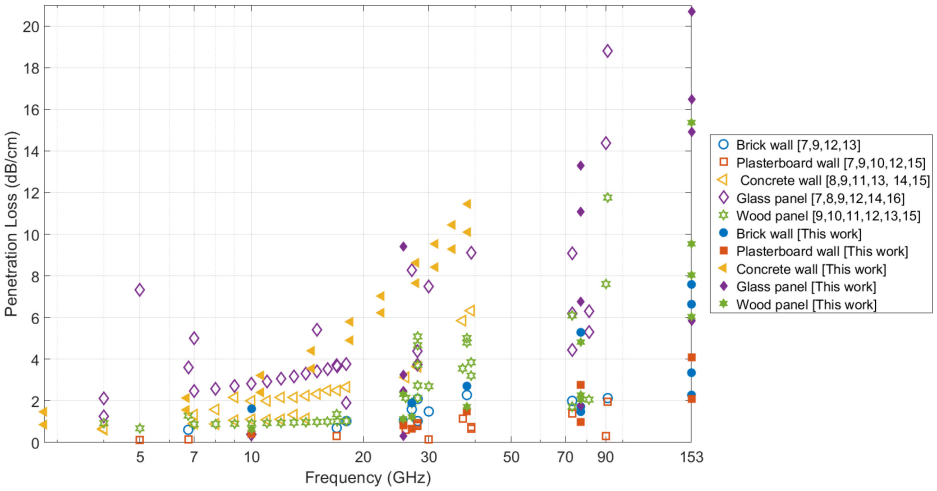

FIGURE 1. Specific Penetration Loss [dB/cm] for different materials from this study and from previous studies.

assumptions. The interaction of waves with materials is governed by three primary propagation mechanisms: transmission (or *penetration*), specular reflection, and diffuse scattering, each influenced by material properties and operating frequency [5], [6]. Previous research has investigated penetration loss across various materials and frequency ranges [7], [8], [9], [10], [11], [12], [13], [14], [15], [16], reflection properties [5], [17], [18], [19], and scattering at 300 GHz [20]. Fig. 1 presents the penetration loss values (dB/cm) for various materials, drawing data from both previous research and this study. Specifically, as it can be observed from Fig. 1, comprehensive studies spanning from the FR3 to sub-THz bands remain scarce. The variability in penetration loss due to differences in the compound composition of common construction materials, such as cement or wood, underscores the need for extensive global measurement campaigns [21]. The variations in Specific Penetration Loss for a given frequency are clearly highlighted in Fig. 1, demonstrating significant variability in materials such as concrete walls and wood panels.

Building on previous research [3], [4], [22], this study investigates material attenuation in common building structures across multiple frequency bands, including 10 GHz, 25.6–28 GHz, 38 GHz, 77 GHz, and 140–153 GHz. The measurement dataset is made available in [23]. The selected frequency bands reflect both currently allocated spectrum and emerging candidate bands for future 6G systems. The 10 GHz band is already identified for International Mobile Telecommunication (IMT) for Region 2 starting from January 2025. The 25.6 GHz and 38 GHz bands fall within the WRC-27 Agenda under Item 1.15 and 1.6 respectively [24]. The 77 GHz band, although primarily allocated for automotive radar applications [25], is increasingly being investigated for short-range high-data-rate communications and integrated sensing and communication (ISAC)—a key research area in 6G. Finally, the 140–153 GHz band lies within the D-band (110–170 GHz), identified by ETSI [26] as a promising candidate for sub-THz indoor access and ultra-dense deployments in 6G networks. Given that common construction materials are inherently composite, inhomogeneous, and highly variable, and that next-generation wireless systems will operate over wide bandwidths, a statistical approach is essential for accurate characterization. This requires multiple measurements across slightly different frequencies within each band, as well as variations in object positioning and sampling times. Additionally, diverse angles of illumination and reception are necessary for an accurate characterization of diffuse scattering. By integrating penetration loss and directional scattering measurements combined with ray-tracing simulations, this study provides an analysis of material attenuation and scattering behaviors. Key characteristics such as penetration attenuation and diffuse scattering parameters are estimated through best-fit procedures. The insights obtained from this study can significantly contribute to the design of next-generation wireless communication systems and improve the reliability of simulation-based planning tools, especially in environments where direct measurements are challenging or unfeasible. The dataset and analysis provided in this work offer a valuable resource for both simulation tool developers and standardization bodies. In particular, the detailed characterization of building materials at the investigated frequencies can be directly incorporated into a ray-tracing software to enhance the modeling of material penetration and scattering. Moreover, the findings can support ongoing standardization efforts targeting high-frequency indoor channel models—such as those in 3GPP TR 38.901 [27] and ITU-R P.2040-3 [28]—by giving empirical data for model refinement under realistic deployment scenarios. The rest of this article is structured as follows: Section II details the measurement setups for each frequency band, Section III presents and discusses the results, and Section IV concludes the study.

II. THE MEASUREMENT SETUP AND PROCEDURE

To characterize the properties of diverse construction materials, penetration (transmission) and diffuse scattering

TABLE 1. Characteristics of the measurement equipment.

Equipment	Model	Measurement parameters
FR3 Band		
VNA	Keysight PNA-X Network Analyzer N5242B	Frequency: 10 MHz - 26.5 GHz
Horn antenna	ARRA X820	Gain: 14-16 dBi
Mm-wave Band		
Transmitter	Custom designed	Frequency: 25.6 GHz, 77 GHz
Receiver	Custom designed Receiver	Frequency : 25.6 GHz, 77 GHz , Sensitivity : -100 dBm
Horn antenna	A-INFO LB-34-20	Gain: 20 dBi
	A-INFO LB-12-10	Gain: 10 dBi
Transmitter	SAF Tehnika J0SSAG14 Signal Generator	Frequency: 26-40 GHz
Receiver	SAF Tehnika J0SSAP14 Spectrum Analyzer	Frequency: 26-40 GHz , Sensitivity: -111 dBm
Circular Horn antenna	SAF Tehnika J0AA2640HG03	HPBW: 12.5°(E-plane), 15°(H-plane)
Sub-THz Band		
Transmitter	Custom designed	Frequency: 153 GHz
Receiver	Custom designed receiver	Frequency : 153 GHz , Sensitivity : -100 dBm
Horn antenna	Mi-Wave 261D-15/387	Gain: 15 dBi
VNA + extenders	Keysight PNA-X Network Analyzer N5242B + WR 6.5	Frequency: 110-170 GHz
Horn antenna	VDI WR-6.5 Conical horn	Gain: 21-23 dBi

measurements were conducted in multiple locations at the University of Bologna (Italy), at Durham University (U.K.), and Universidad Politècnica de Cartagena (Spain). Measurements employed various setups, including Vector Network Analyzer (VNA) - based (with and without frequency extenders) and spectrum analyzer-based setup, with or without a custom-made receiver front-end, as specified in Table 1. In all described measurement setups, the transmitted power was maintained in the 0–20 dBm range. To ensure consistency, some reference, identical materials from the same producer were tested across all setups in all three countries. Moreover, although the setups differ across the three laboratories, the reliability of the results has already been confirmed in previous work, as shown in [29, Sec. 4, Table 6]. This section reports different measurements performed on the same material (paraffin) at the same frequency, showing very good agreement among different setups. Different construction materials and various frequency bands—FR1, FR3, mm-wave, and sub-THz—were investigated in this work, as described in Table 2. A detailed view of the material samples, including the structure of brick holes and the internal and external metal frames of the gypsum board wall, is provided in Fig. 2. The gypsum board wall, as depicted in Fig. 2(c), is shown without its external gypsum layer to enable clear visualization of the internal metallic structure. The materials included in Table 2 are commonly used in buildings construction, and they are likely to continue being employed in the future.

TABLE 2. IUT for each frequency band.

Material	FR1 (0-7 GHz)	FR3 (7-24 GHz)	mm-wave (24 -38 GHz)	sub-THz (110-170 GHz)
Yellow marble	×	✓	✓	×
Brick wall	×	✓	✓	✓
Gypsum board wall	×	✓	✓	✓
Wood flooring	×	✓	✓	✓
Plasterboard	×	✓	✓	✓
Sandstone slab	×	×	✓	×
Plywood	×	×	×	✓
Glass dooor	×	×	×	✓
Wooden door	×	×	×	✓
Indoor partition wall	×	×	×	✓
Plexiglass	×	×	×	✓
Single glass	×	×	×	✓
Double glazed glass	×	×	×	✓
Concrete slab	✓	✓	✓	×
Concrete with metallic mesh	✓	✓	✓	×
Metallic mesh	✓	✓	✓	×

Therefore, investigating the way they interact with the expected, higher communication frequencies is of general interest. Due to variations in available setups and materials at different sites, as well as the difficulty of transporting heavy material samples (*i.e.*, Items Under Test (IUT)), not all materials were characterized at all frequencies. Across all measurement campaigns detailed in this study, the

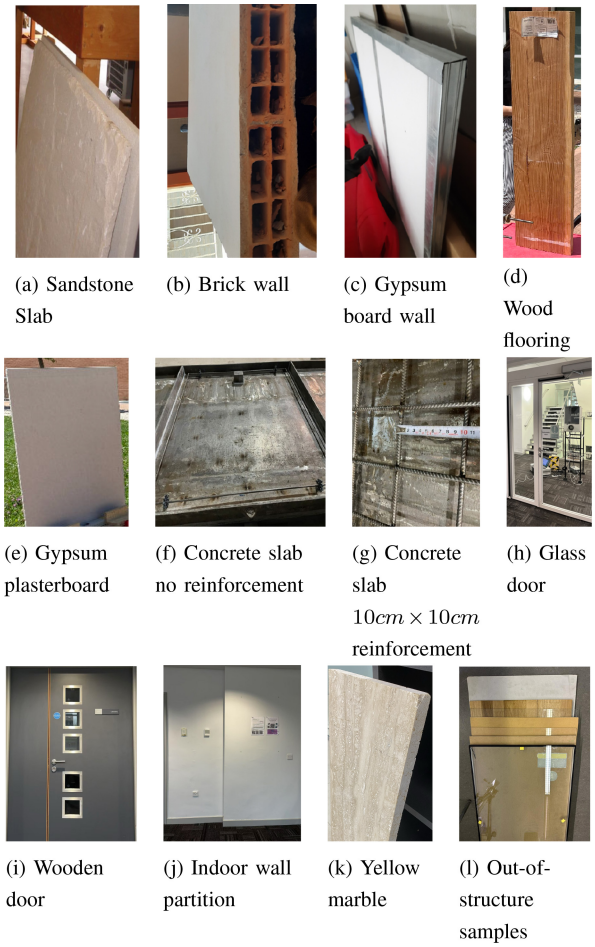

(a) Sandstone Slab (b) Brick wall (c) Gypsum board wall (d) Wood flooring

(e) Gypsum plasterboard (f) Concrete slab no reinforcement (g) Concrete slab $10cm \times 10cm$ reinforcement (h) Glass door

(i) Wooden door (j) Indoor wall partition (k) Yellow marble (l) Out-of-structure samples

FIGURE 2. Detailed view of the materials under test.

(a) Crane holding IUT (b) Absorbers around IUT

FIGURE 3. Measurement procedure.

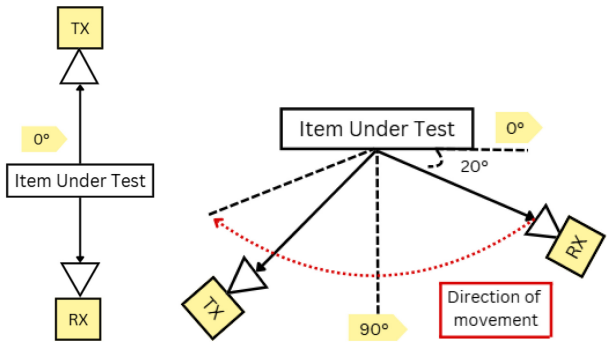

(a) Penetration loss (b) Diffuse scattering

FIGURE 4. Schematic representation of measurement setup principle.

transmitter (TX) and receiver (RX), with directive antennas were consistently mounted at the same height on custom-designed masts, ensuring precise vertical alignment of the antennas. Horizontal alignment between TX and RX was also maintained to target the center of the IUT using laser pointers. Heavy IUTs, such as concrete slabs, were held by a 2000 kg crane and absorbers were placed around the slab to reduce the edge diffraction contribution as depicted in Fig. 3. Moreover, the material samples were sized to exceed the footprint of the TX antenna main beam, to minimize diffraction effects. Vertical polarization was maintained at both ends of the link, ensuring co-polarization between the transmitter and receiver. Regardless of the setup used, two distinctive measurement types were performed, as listed below.

(i) *Penetration loss measurements*. The schematic principle of the penetration loss measurements setup is illustrated in Fig. 4(a). The IUT is placed between the TX and the RX antennas and illuminated with a 0-degree incidence angle. Free-space calibration measurements were performed prior to the insertion of the IUT with the same arrangement to ensure accuracy and eliminate additional losses, such as slight antenna gain imperfections or cable and connector losses. Multiple measurements were performed at slightly different time instants and IUT positions, and the results were then averaged.

(ii) *Scattering measurements*. The setup consists of the IUT illuminated by a transmitting antenna at 135° with respect to the x axis on the slab surface, as shown in Fig. 4(b). The RX, mounted on a pedestal with wheels, is moved across successive points, spaced by 10° on a 140° circular arc (from 20° to 160°). By selecting suitable TX-RX distances and excluding grazing angles in the receiver arc (from 0 to 20° and from 160° to 180°), the entire footprint of the main antenna lobe is ensured to fall entirely within the IUT surface. Free space calibration is performed also in this case, which is necessary for the use of a Ray Tracing model to complement measurements, as shown later in Section III.

It is worth noting that the 135°incidence angle, corresponding to 45° from the x-axis on the surface, was chosen to avoid shadowing caused by the RX antenna in the specular reflection region. With the more usual choice of normal incidence, the RX antenna may partly obstruct illumination of the IUT right when measuring scattering around the specular reflection direction, which is the most important scattering region. We must observe, however, that shadowing is unavoidable in the backward direction, and therefore the back-scattering lobe that has been observed in some materials (e.g., gypsum board wall, see further on) might be affected by measurement inaccuracy.

A. VNA-BASED SETUP

In order to conduct accurate, wideband measurements on construction materials, a VNA is employed in combination with suitable transmitting and receiving antennas for each frequency range, connected through RF cables. Time-gating was performed to select the relevant propagation mechanisms as shown in Section II-C. Prior to each measurement, the VNA is calibrated using a standard calibration kit to ensure accuracy.

FREQUENCY BAND 8-12 GHZ

The first VNA-based measurement campaign conducted at the University of Bologna, Cesena Campus, dealt with wide-band static penetration loss and diffuse scattering measurements in the FR3 band (see details of the considered IUTs in Table 2 and of the measurement equipment in Table 1).

FREQUENCY BAND 1-40 GHZ

The second VNA-based wideband measurement campaign, conducted in Cartagena (Spain), was focused on the penetration loss of concrete slabs, specifically from $1-40\,\text{GHz}$. In particular, two slabs with dimensions $1\,m \times 1\,m \times 0.055\,m$ have been constructed for this measurement campaign. During the construction process, one of the concrete slabs was manufactured with a reinforcement grid with dimensions of $10\,cm \times 10\,cm$ and the other concrete slab was manufactured with no reinforcement (see Fig. 2(f) and Fig. 2(g)). The reinforcing mesh was made with a $7\,mm$ thick iron wire.

FREQUENCY BAND 110-170 GHZ

In order to perform measurements in the sub-THz (D-Band) range, VDI WR6.5 frequency extenders were used in combination to the VNA at both Universities of Bologna and Cartagena. This increased the complexity due to intricate wiring and sensitivity to connector alignment. Therefore, proper calibration is crucial at the start of each measurement campaign to mitigate cable effects.

B. PORTABLE SPECTRUM ANALYZER-BASED SETUP

Portable measurement devices (Signal Generators and Spectrum Analyzers: see Table 1 for specifications) are often preferred over VNAs for their convenience since VNAs are typically bulky, fragile, and require complex calibration. Portable devices can record measurements at a single frequency at a time and directly capture received power, making post-processing straightforward. For these reasons, and for expanding the results of our work across certain frequency ranges, portable measurement devices were used.

FREQUENCY BAND 27 GHZ & 38 GHZ

Static penetration and diffuse scattering measurements were conducted for several materials at these frequencies: yellow marble slab, brick wall, gypsum board wall, sandstone slab, wood flooring and plasterboard. For these measurements, a portable kit provided by SAF Tehnika is utilized, consisting of a Signal Generator [30] and Spectrum Analyzer [31]. Measurement equipment is described in detail in Table 1. A sweep time of 0.5 seconds at the minimum frequency span (two Received Signal Strength values per second can be recorded) is maintained at the Spectrum Analyzer side. Data are averaged over a 10-second interval to mitigate environmental noise.

FREQUENCY BAND 25.6 GHZ, 77 GHZ & 153 GHZ

At Durham (U.K.), a measurement campaign using a custom-designed measurement configuration that can be employed for capturing three frequencies simultaneously is conducted. Our setup utilizes a programmable phase-locked loop (PLL) to generate continuous wave (CW) signals at an intermediate frequency, which is then multiplied by factors of 2, 6, and 12 to produce frequencies of 25.6 GHz, 77 GHz, and 153 GHz, respectively. The 25.6 GHz frequency was specifically selected for comparison with other mm-wave band measurements documented in the literature [32]. The received signals are down converted by a custom designed receiver with a frequency offset to produce beat notes that are then captured by a spectrum analyzer (see Table 1). To minimize measurement errors, four recordings are obtained for each measurement, and the mean value is calculated. To study the impact of indoor structures on signal penetration, the initial focus was on examining materials integrated into the building's structure: a glass door, a wooden door and a main indoor partition wall separating two offices as illustrated in Fig. 2(j). Subsequently, measurements were conducted on various out-of-structure material samples, such as wood flooring, plasterboard, plexiglass, plywood, single glass and double-glazed glass (see Fig. 2(k)). Measurements of materials integrated into the building's structure were straightforward as they were inherently parallel to both TX and RX. Measurements of out-of-structure material samples were performed by the use of a crane (Fig. 3(a)) or of other stable supporting structures.

C. VNA DATA POST-PROCESSING PROCEDURE

After VNA-based measurements for each IUT, proper post-processing was performed in order to extract the power of the main multipath component from the power delay profile (PDP), through the following steps:

- We obtained the channel frequency response (CFR) $H(f)$ across the entire measured frequency band.
- If VNA measurements covered a wide frequency range (e.g., $8-12\,\text{GHz}$ and $110-170\,\text{GHz}$), we divided each entire band into n sub-bands, each characterized by a central frequency and a specific bandwidth over which propagation parameters are assumed to remain constant. The number of sub-bands n is determined based on careful considerations regarding the required time and frequency resolution.

- For each slot, characterized by its own $H(f)$, the Channel Impulse Response (CIR) $h(\tau)$ is derived by applying the Inverse Fourier Transform (IFFT) to the $H(f)$, after it has been appropriately windowed using a Hamming window $W(f)$, as shown in (1).

$$h(\tau) = \mathcal{F}^{-1}\big[W(f) \cdot H(f)\big], \tag{1}$$

where $\mathcal{F}^{-1}$ denotes the inverse Fourier transform. Subsequently, the PDP $P(\tau)$ is given through $h(\tau)$ as:

$$P(\tau) = |h(\tau)|^2. \tag{2}$$

- Finally, an appropriate time gating is applied to the PDP in order to retain only the multipath components relevant for studying either penetration losses or diffuse scattering, depending on the case, as explained below.

III. RESULTS AND DISCUSSION

A. PENETRATION LOSS

1) PENETRATION LOSS ANALYSIS

The penetration loss values at different frequencies and for various IUT were obtained through measurements performed using either a VNA or a Portable Spectrum Analyzer. In both setups, measurements were conducted under two conditions: (i) without the IUT, to serve as a free-space calibration reference, and (ii) with the IUT inserted between the transmitter and receiver. Importantly, both measurements were performed using the same setup configuration, ensuring that any difference in received power can be attributed solely to the presence of the IUT. The penetration loss is calculated as (3):

$$L_{IUT}\ (dB) = P_{LoS} - \sum_{m=1}^{M} \frac{P_m}{M} \tag{3}$$

where L_{IUT} is the penetration loss value of the IUT in dB-unit, P_{LoS} is the received power from free-space calibration, P_m is the m-th received power in obstructed line of sight considering a total of M sampling measurements (where M is at least 10) at slightly different positions of the IUT, and/or for different frequency samples over a total bandwidth of 40 MHz, thus computing the average received power, and therefore mean penetration loss.

2) RESULTS OF PENETRATION LOSS

Table 3 shows the mean penetration loss for normal incidence. The increasing penetration loss versus frequency can be clearly observed. Frequency dependence is well pronounced for brick wall and gypsum board wall (from 13.03 dB at 10 GHz to 53.17 dB at 153 GHz for brick wall; from 2.9 dB at 10 GHz to 32.8 dB at 153 GHz for gypsum board wall). On the contrary, plasterboard, that is lighter and more homogeneous, appears to be less frequency-dependent (from 0.43 dB at 10 GHz to 1.41 dB at 153 GHz). Furthermore, an analysis of the attenuation values' standard deviation (std) was conducted exploiting data over 20 VNA frequency samples, for brick wall and gypsum board wall. Results reported in Table 5 show that no significant fluctuations due to internal resonances within the materials or residual multipath effects were present over the considered bandwidth at all frequencies. To assess precision and repeatability, we repeated selected measurements under different relative positions and/or time instants for reference materials and frequencies, as shown in Table 4. However, due to the extensive and time-consuming nature of the measurements, this analysis was limited to a subset of cases. The resulting *relative standard deviation*, i.e., the ratio of the standard deviation to the mean measured value, remains low, with a maximum of 4.62%.

TABLE 3. Penetration loss values for each frequency band. (Between brackets in blue the comparison with ITU-R P.2040 [28] values for related materials and model in [29]).

Material	Mean Penetration loss [dB]				
	10 GHz	25.6-27 GHz	38 GHz	77 GHz	140-153 GHz
Yellow marble slab (Thickness: 3 cm)	4.86 ("Marble": 2.86)	11.02 (4.15)	17.48 (4.95)	-	-
Brick wall (Thickness: 7 cm)	13.03 ("Brick": 2.98)	15.2 (3.32)	21.7 (3.46)	42.31 (NA)	53.17 (NA)
Gypsum board wall (Thickness: 4 cm)	2.9 (NA)	4.7 (NA)	10.6 (NA)	19.36 (NA)	32.8 (NA)
Wood flooring (Thickness: 4.5 cm)	2.2 (NA)	4.32 (NA)	6.01 (NA)	7.23 (NA)	11.26 (NA)
Plasterboard (Thickness: 1.5 cm)	0.43 (1.64)	2.02 (3.3)	3.01 (4.39)	1.28 (8.01)	1.41 (NA)
Sandstone slab (Thickness: 4 cm)	-	17 (NA)	23 (NA)	-	-
Glass door (Thickness: 1.27 cm)	-	4.12 ("Glass": 4.24)	-	14.08 (11.8)	26.28 (NA)
Wooden door (Thickness: 4.4 cm)	-	10.17 ("Wood": 8.46)	-	21.21 (25.47)	41.97 (NA)
Indoor partition wall (Thickness: 16 cm)	-	17.39 (NA)	-	27.53 (NA)	53.63 (NA)
Plexiglass (Thickness: 4 mm)	-	0.12 (NA)	-	0.71 (NA)	1.14 (NA)
Single glass (Thickness: 4 mm)	-	1.49 ("Glass": 1.98)	-	4.06 (4.94)	5.96 (NA)
Plywood (Thickness: 3 mm)	-	1.35 (1.53)	-	2.73 (1.52)	4.64 (NA)
Double glazed glass (Thickness: 24 mm)	-	13.17 (NA)	-	18.65 (NA)	23.06 (NA)

TABLE 4. Measurement precision expressed in terms of relative std.

Material	Measurement total error			
	27 GHz	38 GHz	77 GHz	153 GHz
Brick wall	1.18 %	-	1.91 %	3.14 %
Yellow marble	4.5 %	4.06 %	-	-
Wood flooring	4.62 %	3.12 %	-	-
Wooden door	1.86 %	-	2.02 %	2.01 %
Glass door	1.45 %	-	3.69 %	2.85 %
Plasterboard	3.46 %	4.32 %	-	-

TABLE 5. Standard deviation analysis considering 20 frequencies samples for selected building materials.

Material	Standard Deviation σ [dB]			
	10 GHz	38 GHz	77 GHz	153 GHz
Brick wall	0.25	0.2	1.17	2.5
Gypsum board wall	0.16	0.03	0.04	0.11

Table 3 provides a comprehensive overview of penetration losses observed across various materials integrated into the buildings' structure (glass door, wooden doors, indoor partition wall) as well as out-of-building material samples. Notably, the glass door demonstrates considerably lower penetration losses compared to its wooden counterpart, with this discrepancy amplifying as frequency increases from 77 to 153 GHz. However, it is important to highlight that, as expected, the penetration losses over all frequencies of the wooden door exceed that of the glass door significantly. It is worth noting that the indoor partition wall, that is made of brick and a layer of white painting, exhibits a penetration loss of 17.39 dB at 25.6 GHz, in alignment with the measured value of the brick wall sample of Fig. 2(b). When considering out-of-structure samples, Table 3 underscores the frequency-dependence of material penetration loss, being higher at 153 GHz than at 25.6 GHz. At 25.6 GHz, the attenuation values of materials match those reported in [32], with plexiglas showing the least attenuation, contrasting with plasterboard which exhibits the lowest attenuation at 77 and 153 GHz.

Since a reference model for penetration loss of construction materials is not available in the literature, we adopt a two-step approach for comparison with our measurements. Specifically, the permittivity and conductivity values provided in [28] of similar reference materials—when available—are used as input to the simple model described in [29, Appendix]. However, real-world building components are typically composite structures, whose attenuation values depend on their specific chemical and physical composition even within the same material group, as illustrated in Fig. 1. Consequently, as shown in Table 3, this two-step model tends to yield results that are not in good agreement with our measurements.

Furthermore, when concrete slabs-with and without reinforcement-are concerned (refer to Fig. 5), the dB-insertion loss seems to increase linearly with frequency. This is reasonable, although the increase with frequency is not as pronounced as suggested by reference formulas [28], where conductivity, attenuation constant, and therefore penetration loss in dB—which are roughly proportional to each other, as explained in [29, Appendix]—are shown to grow exponentially with frequency. Moreover, while the $10\,cm \times 10\,cm$ mesh alone causes negligible attenuation—likely because its size is comparable to or larger than

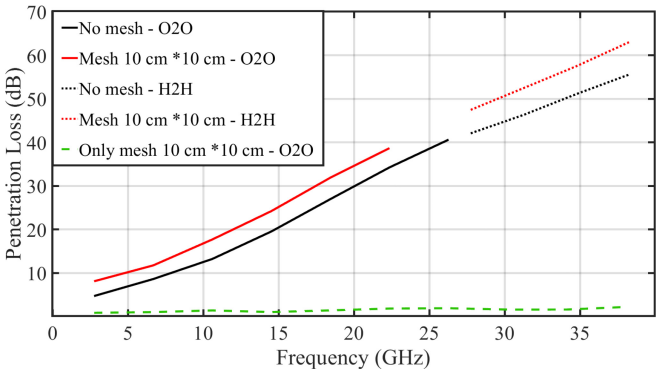

FIGURE 5. Mean penetration loss for two concrete slabs vs. frequency. Solid lines: Omni-to-Omni measurements. Dashed lines: Horn-to-Horn measurements at higher frequencies.

the wavelength at all tested frequencies—the same mesh embedded within the concrete slab results in significantly higher losses: approximately 4 dB at lower frequencies and up to around 8 dB at higher frequencies, compared to the slab without mesh. Resonant or focusing phenomena cannot be invoked to explain such a behavior as results have been averaged both in frequency, over each frequency slot, and in space, over multiple TX antenna and slab positions. According to some accurate measurements with a laser meter, the different concrete slab may display slight thickness undulations that might account for the foregoing attenuation mismatch. However, further investigations on additional, more precise construction samples are necessary to find better interpretation of these results.

In Fig. 1, the Specific Penetration Loss (dB/cm)—computed as the total penetration attenuation of a given material slab divided by the slab's thickness in centimeters—is reported for several materials, as derived from this study and other literature sources. Strictly speaking, total loss is not solely due to through-material attenuation, which depends on thickness, but also results from reflections at the air-medium and medium-air interfaces. Therefore, the use of specific attenuation could be questioned. Nevertheless, it is widely adopted in the literature since it is the only relatively invariant parameter with respect to slab thickness, making it the most effective way to standardize and compare measurements from samples of different thicknesses.

From Fig. 1, we observe that the specific attenuation of almost all materials significantly increases with frequency, except for plasterboard walls, where the increase is relatively mild. Glass panels exhibit the steepest increase and the greater spread, probably due to the large variety of different glass coating.

B. SCATTERING

Scattering measurements were performed using the setup outlined in Section II. Using time-gating when measuring with a VNA, all multipath contributions not originating from the material panel were eliminated. For each scattering measurement, repeatability was verified by performing

independent measurements at different time instants on yellow marble at 27 GHz and 38 GHz, yielding a low relative standard deviation of 1.13% at 27 GHz and 1.21% at 38 GHz. Similarly to what was done in [33] and [34], the results are then compared with ray-tracing simulations performed exactly on the same environment and geometry, following the procedure described below. The radiation patterns of the antennas used in simulations have been measured in a semi-anechoic environment or derived from accurate electromagnetic simulation to minimize simulation errors. The electromagnetic parameters for the different materials were derived from the literature (e.g., [28]) or from measurements performed on the materials themselves as described in [29]. Diffuse scattering was included in ray tracing simulations according to the Effective Roughness (ER) model [33], [35].

It is important to note that, because the ray-tracing simulator operates at a single frequency, the CFR obtained from wideband measurements (after time-gating) was averaged across multiple frequency samples within a narrow band around the center frequency. This was done to minimize fading fluctuations and to obtain a single CFR value to be compared with ray-tracing results. The final objective is to determine the best-match values of the ER model parameters - such as the parameters S and K_R described below - with respect to measurements, therefore characterizing the scattering properties of the materials at different frequencies.

1) DIFFUSE SCATTERING MODELING

The ER model characterizes scattering from building walls due to surface roughness or volume inhomogeneities, assuming that part of the incident power is scattered rather than specularly reflected. The ER model was tuned to align simulated and experimental results. The double-lobe scattering pattern, proposed in [33], is used to represent walls/objects with large volume irregularities and in such a case, the scattered field intensity is expressed as:

$$|\vec{E_s}|^2 = E_{s_0}^2 \left[K_r \left(\frac{1+\cos\psi_R}{2} \right)^{\alpha_R} + (1-K_r) \left(\frac{1+\cos\psi_i}{2} \right)^{\alpha_i} \right] \quad (4)$$

where the amplitude E_{s_0} is proportional to the scattering parameter S (in addition to other factors to ensure power conservation), with S^2 representing the percentage of the reflected power that is spread in non specular directions. ψ_R and ψ_i represent angular deviations from specular reflection and incidence, respectively, while K_R (with $0 < K_R < 1$) governs power distribution between scattering around the specular direction (near-reflection lobe) and back-scattering towards the transmitting direction (back-scattering lobe). α_R and α_i define the width of the reflection and backscattering lobe, respectively. When $K_R = 1$, the scattering pattern boils down to a single-lobe around specular reflection.

2) DIFFUSE SCATTERING PARAMETER CALIBRATION

Table 6 summarizes the calibrated parameters and the Root Mean Square Error (RMSE) between simulated and measured overall power-scattering patterns for all the materials under test. In the following, we analyze the scattering behavior of the different materials, first referring to a single-frequency analysis and then proposing a comprehensive interpretation of the results. As an example, the variation in scattering behavior across different construction materials at the same frequency, 27 GHz, is discussed. Measured and simulated scattering pattern results at 27 GHz are presented in Figures 6a, 6b and 6c for the sandstone slab, the brick wall, and the gypsum board wall, respectively. Except for the sandstone slab, the other two IUTs show the presence of strong back-scattering in RX locations far from specular reflection, probably due to diffraction

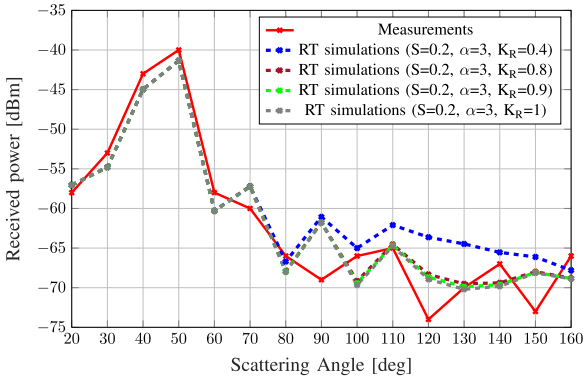

(a) Sandstone slab

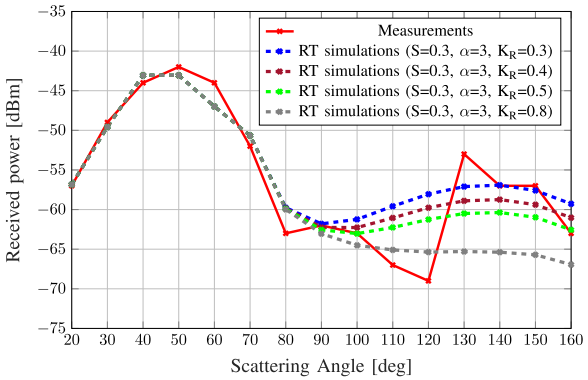

(b) Brick wall

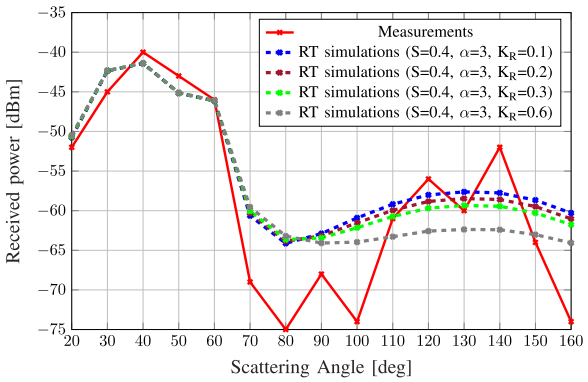

(c) Gypsum board wall

FIGURE 6. Measurement vs simulation comparison for different value of the K_R parameter at 27 GHz.

TABLE 6. Best-fit parameters of ER Scattering Model in the backward scattering case at 10, 27, 38 and 140 GHz.

Material	10 GHz			27 GHz			38 GHz			140 GHz		
	Best-fit S	*Best-fit* K_R	*RMSE*	*Best-fit S*	*Best-fit* K_R	*RMSE*	*Best-fit S*	*Best-fit* K_R	*RMSE*	*Best-fit S*	*Best-fit* K_R	*RMSE*
Brick wall	0.3	0.5	4.22	0.3	0.5	3.24	0.4	0.9	5.43	0.3	1	4.21
Plasterboard	0.1	0.5	3.05	0.4	0.7	6.93	0.4	0.8	5.08			
Yellow marble slab	0		5.91	0.1	0.9	6.4	0.1	0.9	4.68			
Sandstone slab				0.2	1	3.24	0.1	0.9	8.6			
Gypsum board wall	0.5	0.5	6.28	0.4	0.3	6.42	0.5	0.2	5.34	0.5	0.5	4.6
Wood flooring	0.5	0.5	4.6	0.2	0.6	7.36	0.1	0.9	6.91			

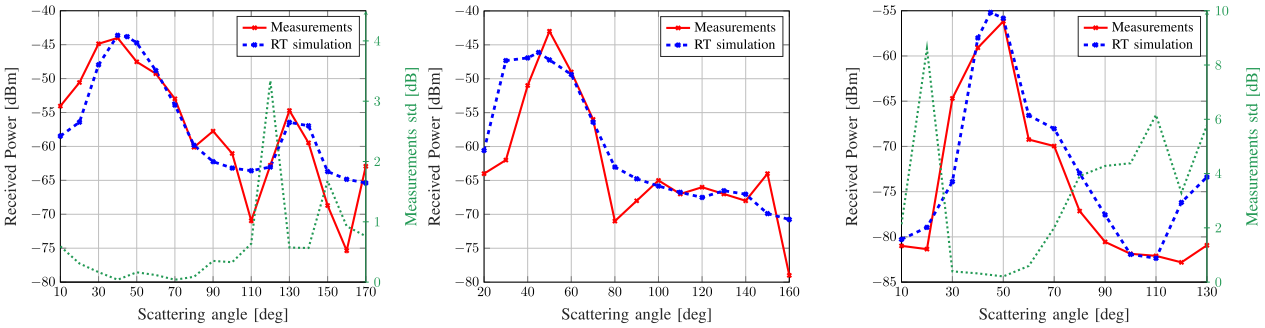

(a) 10 GHz (b) 38 GHz (c) 140 GHz

FIGURE 7. Brick wall sample: measurements vs simulation at different frequencies. The red curve represents the average measured received power around the considered frequency, while the green curve represents the standard deviation. The blue curve shows the simulation results.

and back-reflection effects caused by the samples' internal structures. This finding is supported by the fact that the double-lobe scattering pattern proposed in [33] and defined by (4) provides the best results in both cases. The key parameters of the ER model were calibrated to closely match measurements, with the angular amplitude fixed at $\alpha_R = \alpha_i = 3$, based on previous studies on similar building materials [33], [36]. The parameter K_R (referred to as L in [33]) was 0.5 for the brick wall, indicating equal diffuse power in both lobes and 0.3 for the gypsum board wall, with 70% of power directed towards back-scattering. On the other hand, K_R is equal to 1 for sandstone, which means, there is no relevant backward diffuse scattering in this case. Correspondingly, the scattering parameter S showed that gypsum board walls generated the relatively strongest diffuse scattering. These results show that volume scattering is quite relevant and becomes severe for light, low-loss materials with internal inhomogeneities such as the gypsum board. The main origin of diffuse scattering in the considered cases cannot be surface roughness since all three materials have similar, smooth surfaces. It is worth noting that the best-fit RMSE, low for the first two cases, is sensibly higher for the gypsum board, due to the deep saddle of the curve between 80 and 100 degrees, which the ER model cannot reproduce well. Probably, the Effective Roughness model is not very suitable to describe such a directive scattering, that might be properly reproduced using deterministic ray tracing on the base of an accurate description of the internal reinforcement structure. The internal structure, however, is often a-priori unknown. Alternatively, new version of the ER model with a different formulation could be proposed. Such a new formulation will have to satisfy reciprocity and power balance and therefore will require an entirely new mathematical derivation, that can only be addressed in a future dedicated paper.

With reference to Table 6, a comprehensive interpretation of the results is presented, highlighting the relationship between material irregularities, frequency and the importance of surface-generated vs. volume-generated diffuse scattering. Since as frequency increases penetration becomes less important, the material portion contributing to volume-generated scattering becomes thinner and closer to the surface. Consequently, volume inhomogeneities contribute more to scattering at lower frequencies, with a pronounced two-lobe pattern as volume irregularities can generate backward-scattering due to a "billiard" effect [33], while surface roughness plays a more relevant role at higher frequencies and produces only a forward lobe around the specular reflection direction. This means that materials with a homogeneous volume but irregular surface should exhibit more pronounced diffuse scattering as the frequency increases, resulting in an increasing S parameter with frequency, whereas materials with an irregular volume but smooth surface should exhibit stronger scattering at lower frequencies. As evident from Table 6, the marble slab and plasterboard—both characterized by volumetric homogeneity—exhibit an increasing trend in the scattering coefficient S with frequency, along with high K_R values. In contrast, the wooden flooring, which presents significant internal irregularities due to the natural wood grain, shows a decreasing S with increasing frequency. As for the brick wall, its characteristics are intermediate between the two foregoing cases, and therefore its parameters float up and down with frequency without a clear trend. Fig. 7 explicitly shows the

comparison between measurements and simulations for the brick wall: the gradual decrease in the backward lobe at around 135° is probably related to the above-mentioned attenuation of volume-scattering at high frequencies, that also reflects in the increasing values of K_R in Table 6. The standard deviation over multiple frequency samples (20 in both cases) is also shown in Fig. 7 for cases (a) and (c) that were measured using a VNA setup: it is very low in the specular lobe, where specular reflection is the dominant contribution, while it is higher away from it. This fact confirms that diffuse scattering is the effect of multiple micro-contributions that generate some sort of fading in the frequency domain. Other materials containing various types of components, such as the gypsum board wall, which also includes metal studs within its structure, exhibit parameters that vary with frequency in a way that is not easily predictable. In any case, for the gypsum board wall, the K_R values are quite low, indicating a strong back-scattering contribution due to volumetric irregularities, while S remains almost constant with frequency.

IV. CONCLUSION

This study examines the attenuation and scattering characteristics of common construction materials at frequencies from 10 to 153 GHz, using appropriate measurement setups and post-processing techniques. First of all, penetration loss for some of the most common construction material slabs is characterized, highlighting the strong increase with frequency for some materials, e.g., glass panels and brick wall, and the mild one for plasterboard and other materials. In all cases, standard deviation over different frequency samples around the considered center frequency is very small. In addition, scattering from some common construction materials at multiple frequencies is analyzed through both directional measurements and ray tracing simulations. Differently from common sentiment, it is shown that scattering from internal structures can be relevant even at mm-wave frequencies, especially in the case of Gypsum-board dividing-walls which have a low penetration loss and relevant internal inhomogeneities. Results also show that probably, a different model with a more directive back-scattering lobe should be used in the Effective Roughness scattering model for this case. Backward diffuse scattering is also evident for the brick wall, that together with gypsum board wall represents by far the most common type of dividing wall worldwide. Our findings can contribute to the design of future communication systems and to the calibration of propagation simulators essential for their real-world deployment and optimization. Future work will have to address higher frequencies in the sub-THz range, which are relevant to next-generation wireless systems, and to evaluate how variations in compound materials among different manufacturers may influence both penetration and scattering characteristics. Additionally, expanding the material database to include more modern and complex building materials will enhance the applicability of future propagation models.

REFERENCES

[1] S. Kang et al., "Cellular wireless networks in the upper mid-band," *IEEE Open J. Commun. Soc.*, vol. 5, pp. 2058–2075, 2024.

[2] *Agenda Item 1.7 WRC-27, Terrestrial Mid-Band IMT*, Int. Telecommun. Union, Geneva, Switzerland, Accessed: Jun. 2025.

[3] S. Kodra, J. Hu, M. Barbiroli, V. Degli-Esposti, and S. Salous, "Multi-frequency measurements of material and floor penetration losses," in *Proc. 4th URSI Atlant. RadioSci. Conf.*, 2024, pp. 1–4.

[4] S. Kodra, M. Barbiroli, E. M. Vitucci, F. Fuschini, and V. Degli-Esposti, "Mm-Wave building penetration losses: A measurement-based critical analysis," *IEEE Open J. Antennas Propag.*, vol. 5, pp. 404–413, 2024.

[5] Y. Wang et al., "Measured reflection and transmission properties of building materials for indoor THz communication," *IEEE Antennas Wireless Propag. Lett.*, vol. 22, pp. 1361–1365, 2023.

[6] A. A. Ayeni, A. A. Yusuf, and S. O. Onidare, "Correlation between the electromagnetic properties of building materials and wireless signal penetration loss," *IEEE Trans. Antennas Propag.*, vol. 70, no. 12, pp. 12040–12048, Dec. 2022.

[7] D. Bonefačić and L. Šarolić, "Attenuation of building materials and structures in 5G millimeter wave band," in *Proc. 17th Eur. Conf. Antennas Propag. (EuCAP)*, 2023, pp. 1–5.

[8] D. W. Matolak, M. Mohsen, and J. Liu, "Building material attenuations at 5 GHz and at mmWave frequencies 30 GHz and 90 GHz," in *Proc. IEEE 21st Annu. Wireless Microw. Technol. Conf. (WAMICON)*, 2021, pp. 1–4.

[9] N. Hosseini et al., "Attenuation of several common building materials: Millimeter-wave frequency bands 28, 73, and 91 GHz," *IEEE Antennas Propag. Mag.*, vol. 63, no. 6, pp. 40–50, Dec. 2021.

[10] C. E. O. Vargas and L. d. S. Mello, "Measurements of reflection and penetration loss of construction materials at 28 GHz and 38 GHz," in *Proc. IEEE-APS Topical Conf. Antennas Propag. Wireless Commun. (APWC)*, 2018, pp. 897–900.

[11] H. Lee, H. Kim, H. Chung, K. Cha, and S. Kim, "Penetration loss analysis for mmWave MIMO communication in indoor environments," in *Proc. 14th Int. Conf. Inf. Commun. Technol. Converg. (ICTC)*, 2023, pp. 1039–1041.

[12] M. Niedźwiecki, M. Zawadzki, and K. Cichoń, "Measurements of material loss and floor penetration for 18–30 GHz," in *Proc. 25th Int. Microw. Radar Conf. (MIKON)*, 2024, pp. 70–74.

[13] M. Quispe, J. Samaniego, J. Olivares, M. Chuchón, M. Becerra, and S. Inca, "Transmission loss analysis of indoor building materials in the 24–30 GHz frequency range," in *Proc. IEEE 31st Int. Conf. Electron., Elect. Eng. Comput. (INTERCON)*, 2024, pp. 1–6.

[14] M. Khatun, C. Guo, D. Matolak, and H. Mehrpouyan, "Indoor and outdoor penetration loss measurements at 73 and 81 GHz," in *Proc. IEEE Global Commun. Conf. (GLOBECOM)*, 2019, pp. 1–5.

[15] D. Shakya et al., "Comprehensive FR1(C) and FR3 lower and upper mid-band propagation and material penetration loss measurements and channel models in indoor environment for 5G and 6G," *IEEE Open J. Commun. Soc.*, vol. 5, pp. 5192–5218, 2024.

[16] Y. C. Lee, S.-S. Oh, C. W. Byeon, K. Aziding, and B.-L. Cho, "Impact of window penetration loss on building entry loss from 3.5 to 24 GHz," *IEEE Access*, vol. 9, pp. 138571–138579, 2021.

[17] Y. Geng, V. Yajnanarayana, A. Behravan, E. Dahlman, and D. Shrestha, "Study of reflection-lass-based material identification from common building surfaces," in *Proc. Joint Eur. Conf. Netw. Commun. 6G Summit (EuCNC/6G Summit)*, 2021, pp. 526–531.

[18] M. A. Aliouane, J.-M. Conrat, J.-C. Cousin, and X. Begaud, "Material reflection measurements in centimeter and millimeter wave ranges for 6G wireless communications," in *Proc. Joint Eur. Conf. Netw. Commun. 6G Summit (EuCNC/6G Summit)*, 2022, pp. 43–48.

[19] Y. Wang, Y. Liu, X. Liao, Z. Yu, G. Wang, and J. Zhang, "Complex permittivity extraction of building materials from transmission/reflection measurements at sub-THz band," in *Proc. IEEE Globecom Workshops (GC Wkshps)*, 2023, pp. 1934–1939.

[20] F. Taleb, G. G. Hernandez-Cardoso, E. Castro-Camus, and M. Koch, "Transmission, reflection, and scattering characterization of building materials for indoor THz communications," *IEEE Trans. Terahertz Sci. Technol.*, vol. 13, no. 5, pp. 421–430, Sep. 2023.

[21] A. Asp, T. Hentilä, M. Valkama, J. Pikkuvirta, A. Hujanen, and I. Huhtinen, "Impact of different concrete types on radio propagation: Fundamentals and practical RF measurements," in *Proc. 4th Int. Conf. Smart Sustain. Technol. (SpliTech)*, 2019, pp. 1–8.

[22] E. M. Vitucci, M. Buccioli, and V. Degli-Esposti, "Analysis of mm-wave scattering from construction materials," in *Proc. URSI GASS*, Rome, Italy, Sep. 2021, pp. 2–6.
[23] (Zenodo, Geneva, Switzerland). *6G SHINE Proejct*. Accessed: Jun. 2025. [Online]. Available: https://www.zenodo.org/communities/6g-shine/records?q=&l=list&p=1&s=10&sort=newest
[24] "Agenda Items WRC-27." Accessed: Jun. 2025. [Online]. Available: www.cept.org/ecc/groups/ecc/cpg/page/agenda-for-wrc-27
[25] (ComSoc, Piscataway, NJ, USA). *IEEE Communications Technology News: Sensing, Communications or Sensing and Communications? Perhaps both Together*. Accessed: Jun. 2025. [Online]. Available: https://www.comsoc.org/publications/ctn/sensing-communications-or-sensing-and-communications-perhaps-both-together
[26] *Terahertz Technology; Identification of Frequency Bands of Interest for THz Communication Systems*, ETSI Standard GR THz 002 V1.1.1, Mar. 2024.
[27] "5G; Study on channel model for frequencies from 0.5 to 100 GHz; (Release 16), Version 16.1.0," 3GPP, Rep. TR 138 901, Nov. 2020.
[28] *Effects of Building Materials and Structures on Radiowave Propagation Above About 100 MHz*, ITU-Rec. P.2040-3, Int. Telecommun. Union, Geneva, Switzerland, Aug. 2023.
[29] L. Possenti et al., "Improved fabry-pérot electromagnetic material characterization: Application and results." *Radio Sci.*, vol. 55, no. 11, 2020, Art. no. e2020RS007164.
[30] "SAF Tehnika signal generator website." Accessed: Jun. 2025. [Online]. Available: https://spectrumcompact.com/
[31] "SAF Tehnika spectrum analyzer website." Accessed: Jun. 2025. [Online]. Available: https://www.saftehnika.com/en/ebandspectrum compact
[32] S. El Faitori and S. Salous, "Reflection and penetration loss wideband measurements of building materials at 28 GHz and 39 GHz," in *Proc. 16th Eur. Conf. Antennas Propag. (EuCAP)*, 2022, pp. 1–4.
[33] V. Degli-Esposti, F. Fuschini, E. M. Vitucci, and G. Falciasecca, "Measurement and modelling of scattering from buildings," *IEEE Trans. Antennas Propag.*, vol. 55, no. 1, pp. 143–153, Jan. 2007.
[34] J. Pascual-García, J.-M. Molina-García-Pardo, M.-T. Martínez-Inglés, J.-V. Rodríguez, and N. Saurín-Serrano, "On the importance of diffuse scattering model parameterization in indoor wireless channels at mm-Wave frequencies," *IEEE Access*, vol. 4, pp. 688–701, 2016.
[35] E. M. Vitucci, N. Cenni, F. Fuschini, and V. Degli-Esposti, "A reciprocal heuristic model for diffuse scattering from walls and surfaces," *IEEE Trans. Antennas Propag.*, vol. 71, no. 7, pp. 6072–6083, Jul. 2023.
[36] F. Fuschini et al., "Item level characterization of mm-Wave indoor propagation," *EURASIP J. Wireless Commun. Netw.*, vol. 2016, p. 4, Jan. 2016.

SILVI KODRA received the first M.Sc. degree in telecommunications engineering from the University of Bologna, the second M.Sc. degree in electronics and communication engineering from Tongji University, Shanghai, and the Ph.D. degree in telecommunications engineering from the University of Bologna in March 2025. She has served as the Young Researcher Representative for COST CA20120 Interact from 2024 to 2025. Her activity is focused on the research topic in reconfigurable intelligent surfaces, channel characterization for mm-wave and sub-THz frequencies, and propagation losses in indoor environments. She is currently involved as the student chair in the organization of several conferences.

ELENA BERNARDI (Graduate Student Member, IEEE) received the B.S. degree in electronics engineering and the M.S. degree in electronics and telecommunications engineering from the University of Bologna, Italy, in 2019 and 2022, respectively, where she is currently pursuing the Ph.D. degree in electronics, telecommunications, and information technologies engineering. Since 2022, she has been with the National Inter-University Consortium for Telecommunications, Wireless Laboratory, working on massive multiple access and channel characterization at mmWave and sub-THz. Her research interests include channel propagation analysis, measurements across different propagation environments, ray tracing, and reconfigurable intelligent surfaces.

NICOLÒ CENNI (Graduate Student Member, IEEE) received the B.Sc. and M.Sc. degrees in electronics and telecommunications engineering from the University of Bologna, Italy, in 2021 and 2023, respectively, where he is currently pursuing the Ph.D. degree in electronics, telecommunications, and information technologies engineering. His research interests include wave propagation phenomena, such as diffraction and diffuse scattering, ray-tracing simulations, and ray-based modeling of reconfigurable intelligent surfaces.

JIAHAO HU received the B.S. degree in electronic and information engineering from the Shanghai University of Engineering Science, Shanghai, China, in 2021, and the M.Sc. degree in electrical engineering from Durham University, Durham, U.K., in 2022, where he is currently pursuing the Ph.D. degree with the Communication and THz Node, under the supervision of Prof. S. Salous. His research interests include millimeter-wave and terahertz propagation measurements, channel modeling, and rain attenuation in the millimeter-wave and terahertz bands.

MARINA BARBIROLI received the Laurea degree in electronic engineering and the Ph.D. degree in computer science and electronic engineering from the University of Bologna in 1995 and 2000, respectively, where she is currently an Associate Professor with the Department of Electrical, Electronic and Information Engineering "G. Marconi." Her research focuses on radio systems designing through theoretical and experimental modeling of the wireless propagation channel. Her research activity includes the participation to European research and cooperation programs.

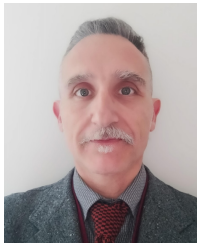

FRANCO FUSCHINI received the M.Sc. degree in telecommunication engineering and the Ph.D. degree in electronics and computer science from the University of Bologna, Italy, in March 1999 and July 2003, respectively, where he is currently an Associate Professor with the Department of Electrical, Electronic and Information Engineering "Guglielmo Marconi." He is the author or co-author of more than 50 journal articles on electromagnetic wave propagation and wireless systems design. His main research interests are in the area of radio systems technologies and radio propagation theoretical modeling and experimental investigation. In April 1999, he received the "Marconi Foundation Young Scientist Prize" in the context of the XXV Marconi International Fellowship Award.

ENRICO MARIA VITUCCI (Senior Member, IEEE) is currently an Associate Professor of Applied Electromagnetics, Antennas, and Propagation with the Department of Electrical, Electronic and Information Engineering "G. Marconi," University of Bologna. Previously, he was a Research Associate with the Center for Industrial Research on ICT, University of Bologna. In 2015, he was a Visiting Researcher with Polaris Wireless, Inc., Mountain View, CA, USA. He is the Chair of the Cesena-Forli Unit, Inter-Department Center for Industrial Research on ICT (CIRI-ICT), University of Bologna. He is the author or co-author of about 100 technical articles on international journals and conferences, and a co-inventor of five international patents. He participated to several European research and cooperation programs (COST 2100, COST IC1004, COST IRACON, and COST INTERACT) and in the European Networks of Excellence NEWCOM and NEWCOM++. His research interests are in deterministic and wireless propagation models for 5G and beyond. He is a member of the Editorial Board of *Wireless Communications and Mobile Computing*.

JOSE-MARIA MOLINA GARCIA-PARDO received the telecommunications engineering degree from the Universidad Politécnica de Valencia, Spain, in 2000, the M.Sc. degree in communication and signal processing in Newcastle upon Tyne, U.K., in September 2001, and the Ph.D. degree in telecommunications and the bachelor's degree in business and administration from the Universidad Politécnica de Cartagena (UPCT), Spain, in 2004 and 2008, respectively. He is a Distinguished Professor with the University of Lille. In 2001, he joined the Department of Information Technologies and Communications, UPCT, where he has been an Associate Professor since 2007, a Full Professor accredited in 2012, and a Full Professor since 2016. He leads the SiCoMo Research Group. He is the lead researcher in some national projects and participates actively in the European COST Action INTERACT. He is an author of more than 120 journals indexed in the JCR, more than 300 international conferences, five book chapters, and owes four patents related to telecommunications. His research activities are centered on radio-communications, propagation, channel modeling, and experimental channel sounding in different frequency bands (400 MHz–300 GHz) and technologies (GSM, UMTS, LTE, 5G, 6G, WiFi, WSN, TETRA, mmW, OFDM, MIMO, BAN, and cognitive radio).

MARÍA-TERESA MARTÍNEZ-INGLÉS received the degree in telecommunications engineering and the master's (research) degree in information and communication technologies from the Universidad Politécnica de Cartagena (UPCT), Spain, in 2009 and 2011, respectively, and the joint Doctoral degree from the University of Lille 1, France, in the *Micro et Nano Technologies, Acoustique et Télécommunications* Program in October 2014, receiving the Extraordinary Doctorate Award. In December 2011, she began her Ph.D. studies as an FPI (Research Personnel in Training) Fellow with the Official Doctoral Program in Information and Communication Technologies, Department of Information Technologies and Communications, UPCT. In February 2016, she was appointed as an Assistant Lecturer with the Centro Universitario de la Defensa de San Javier, affiliated with UPCT, where she has been an Associate Professor since August 2019. She obtained the national accreditation for Full Professor in October 2020. She is a member of the Sistemas de Comunicaciones Móviles (SICOMO) Research Group, UPCT. She has participated in seven competitive R+D+I projects and is the author of more than 30 scientific papers published in JCR-indexed journals. Her research activity focuses on the analysis, modeling, and characterization of the radio propagation channel in 5G frequency bands, particularly in the millimeter-wave spectrum. In October 2015, she was also honored by the Official College and the Spanish Association of Telecommunication Engineers with the Yoigo Award for the Best Ph.D. Thesis in High-Speed Broadband Mobile Communications.

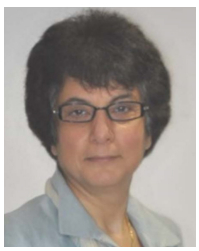

SANA SALOUS (Senior Member, IEEE) received the B.E.E. degree from the American University of Beirut, Beirut, Lebanon, in 1978, and the M.Sc. and Ph.D. degrees from Birmingham University, Birmingham, U.K., in 1979 and 1984, respectively. She was an Assistant Professor with Yarmouk University, Irbid, Jordan, for four years followed by a one-year Research Fellowship with Liverpool University, Liverpool, U.K. She held a lectureship with the University of Manchester Institute of Science and Technology, Manchester, U.K., in 1989, where she was subsequently a Senior Lecturer and then a Reader. Since 2003, she has been the Chair of Communications Engineering with Durham University, Durham, U.K., where she is currently the Director of the Centre for Communication Systems. Her current research interests include radio channel characterization in various frequency bands ranging from skywave in the HF band to millimeter-wave bands, design of radar waveforms, and novel radio channel sounders and radar systems for radio imaging. She was the Chair of the Commission C on Radio Communication and Signal Processing Systems of URSI from 2014 to 2017 and is currently a member of the Board of URSI. She was the Editor-in-Chief of *Radio Science* (American Geophysical Union) from 2019 to 2025.

VITTORIO DEGLI-ESPOSTI (Senior Member, IEEE) is a Full Professor with the "Dipartimento di Ingegneria Elettrica, Elettronica e dell'Informazione," Alma Mater Studiorum - Università di Bologna. From January 2015 to December 2016, he was the Director of Research with Polaris Wireless Inc., Mountain View, CA, USA. In 1998, he was a Postdoctoral Researcher with Polytechnic University (currently NYU Tandon School of Engineering), Brooklyn, NY, USA, in the group led by Prof. H. L. Bertoni. He has been a Visiting Professor with the Helsinki University of Technology (currently Aalto University) and Tongji University, Shanghai, in 2006 and 2013, respectively, and participated in several European research projects, including many European Cooperation Actions (COST), the European Networks of Excellence NEWCOM and NEWCOM++, and other 7th framework and Horizon Europe projects. He is a Mercator Fellow of the Deutsche Forschungsgemeinschaft (DFG), in affiliation with the 4-CAD Project. He has been the Chair of the Propagation Working Group of the European Association on Antennas and Propagation (EuRAAP) and of WG1 of COST Action CA20120 "Interact." He has been the Vice-Chair of the European Conference on Antennas and Propagation (EuCAP), editions 2010 and 2011, the Short-Courses and Workshops Chair of the 2015 edition, the Convened Sessions Chair of the 2023 edition, an Invited Speaker at EuCAP 2014 and the International Symposium on Antennas and Propagation (ISAP) 2020, and the Short-Courses Chair of the European Conference on Networks and Communications (EuCNC) 2020. He has been the Co-Founder and a Lecturer of the biennial Courses for Ph.D. students and researchers "Short-Range Radio Propagation" and "Mobile Radio Propagation for 5G and Beyond" of the European School of Antennas. He is the author or co-author of over 170 peer-reviewed technical papers and a co-inventor of seven international patents in the fields of applied electromagnetics, radio propagation, and wireless systems. He has been a recipient of the "2023 EurAAP Propagation Award." He is an Editor of the IEEE TRANSACTIONS ON VEHICULAR TECHNOLOGY.